DEVELOPMENT OF A FIBER BASED ENDOSCOPE FOR ULTRASOUND INDUCED OPTICAL COHERENCE ELASTOGRAPHY

The text does not wrap; each field must be entered individually.

By

Karndeep Singh Rai-Bhatti

A capstone project submitted for
Graduation with University Honors

June 6, 2018

University Honors
University of California, Riverside

APPROVED

_____

Dr. B. Hyle Park
Department of Bioengineering

_____

Dr. Richard Cardullo, Howard H Hays Jr. Chair and Faculty Director, University Honors
Interim Vice Provost, Undergraduate Education

Abstract

There are an estimated 3 million cases of osteoarthritis in the U.S. every year[1]. Osteoarthritis is characterized by the degeneration of cartilage which leads to joint pain and reduced range of motion. Currently there are a limited number of methods for diagnosis and monitoring of osteoarthritis that can only detect the disease after serious deterioration has already occurred. To produce a higher resolution, higher magnification image of the joint tissue, we propose to insert a needle-based endoscope in a procedure that would mirror that of a joint aspiration. The endoscope will serve as the sample arm of an Optical Coherence Tomography (OCT) system. We intend to utilize the OCT system in conjuncture with an ultrasound transducer to both produce images of cartilage while also quantifying its mechanical properties by using a technique known as Optical Coherence Elastography (OCE). We successfully assembled a micro-endoscope composed of two 350 μm lenses attached to a 300 μm prism with a fixed focal length of approximately 1.5 mm. Light was successfully passed through our device and received back with a net power loss of 5 dB. A supporting system of rotational and translation motors with encoders was constructed and programmed to move and monitor the position of the endoscope as well as allow for reconstruction of the image through post imaging processing code. All components were synchronized using the OCT system's trigger output. This device has potential to be a valuable tool for clinicians in orthopedics and has potential to improve a virtually non-existent market for imaging osteoarthritis.

Acknowledgments

I would like to that my faculty mentor, Dr. Hyle Park, and all the members of NOIR labs.

Table of Contents

1. Introduction

Osteoarthritis currently affects 27 million adults. It is the leading cause of joint disorders and most common cause of disabilities among adults in the United States. It is projected that this statistic will rise to 67 million by the year 2030. While this condition affects approximately 10% of men and 13% of women above the age of 60, symptoms and effects can begin to develop as early as one's mid-twenties[3]. The condition itself is a disease of the synovial joints and leads to the mechanical degeneration of cartilage tissue. Currently, methods of diagnosis include: synovial fluid extracts, X-ray imaging, and Magnetic Resonance Imaging (MRI). Chondrocytes uphold joint integrity by maintaining a delicate balance of cytokines, growth factor signals, and physical stimuli. When this balance is disrupted, cartilage matrix degradation is initiated and fragments will accumulate in the synovial space. A synovial fluid extraction samples the fluid in the synovial space and can be tested for indicators of damage. While this gives clinical practitioners an idea of the progression of the disease, there is no quantitative assessment of the actual damage to the cartilage tissue. MRI allows for good resolution and full depth imaging, but is expensive and has a significant delay between images being taken and results. X-ray imaging has good depth penetration, but produces relatively lower resolution images and requires that the patient be exposed to radiation.

To better image and monitor the health and mechanical properties of any given joint, we propose to image the interior of joints utilizing a micro-endoscope. It will utilize both optical coherence tomography (OCT) and ultrasound to both measure the mechanical properties while also producing a cylindrical volumetric image. High-resolution images can be generated with axial resolution as high as 10μm. Comparable resolutions are not obtainable when utilizing other conventional imaging systems such as Magnetic Resonance Imaging(MRI) and X-rays. An

adaptation of OCT we are looking to utilize is optical coherence elastography (OCE). OCE is a novel technology that allows for the analysis of biomechanical properties of tissues. In conjunction with ultrasound, OCE can be used to determine the mechanical properties of our tissue of choice: cartilage[5]. The articular cartilage within the knee joint experiences an increase in stiffness due to the progression of osteoarthritis. As shown by Manickam et al., ultrasound technology can be used to distinguish between different stiffness's of varying agar samples[6]. We are proposing to use OCE as a diagnostic tool for osteoarthritis. Ultimately, ultrasound perturbation will be used to vibrate the cartilage sample and evaluate the differences in stiffness between osteoarthritic cartilage and non-osteoarthritic cartilage via OCT imaging. Initial testing of the design will be done in a rat model. We hope to be able to monitor the progression of osteoarthritis in the rat's knee joint as well as monitor the progression of possible treatments and use our endoscope as a new research instrument.

2. Design Documentation

2.1 Design of the Endoscope

The endoscope is made of multiple components housed within a 21-gauge needle. It serves as the sample arm to a spectral domain OCT system with light centered at 1310 nm. Light is sent through SMF28 Ultra Optical Fibers by Corning. Prior to gluing, the fiber's protective sheath is cleaved. The fiber is then glue to 2 Gradient-Index (GRIN) lenses purchased from Edmunds Optics. Each has 350 μm diameter, with a tolerance of 10μm, and a length of 780 μm, with a tolerance of +/- 5%. Each lens is a quarter pitch, so to ensure light focusing at the desired focal length, two lenses had to be glued together. They were then ground down to the desired focal length. To redirect the light out of the endoscope, a 300 μm aluminum coated right angle prism was glued to the end of the two prisms. A needle ground into a trough using a Dremel was

used to align the lenses and act as a backbone to the endoscope. The whole assembly was inserted into a 21-gauge needles from TERUMO and glued in place. A 0.3 mm hole was drilled into the side of the needle to serve as a window for light to pass through. The window was sealed shut using optically clear UV-curing Optical Adhesive NOA81. Lenses, the prism and fiber were all adhered with the same adhesive.

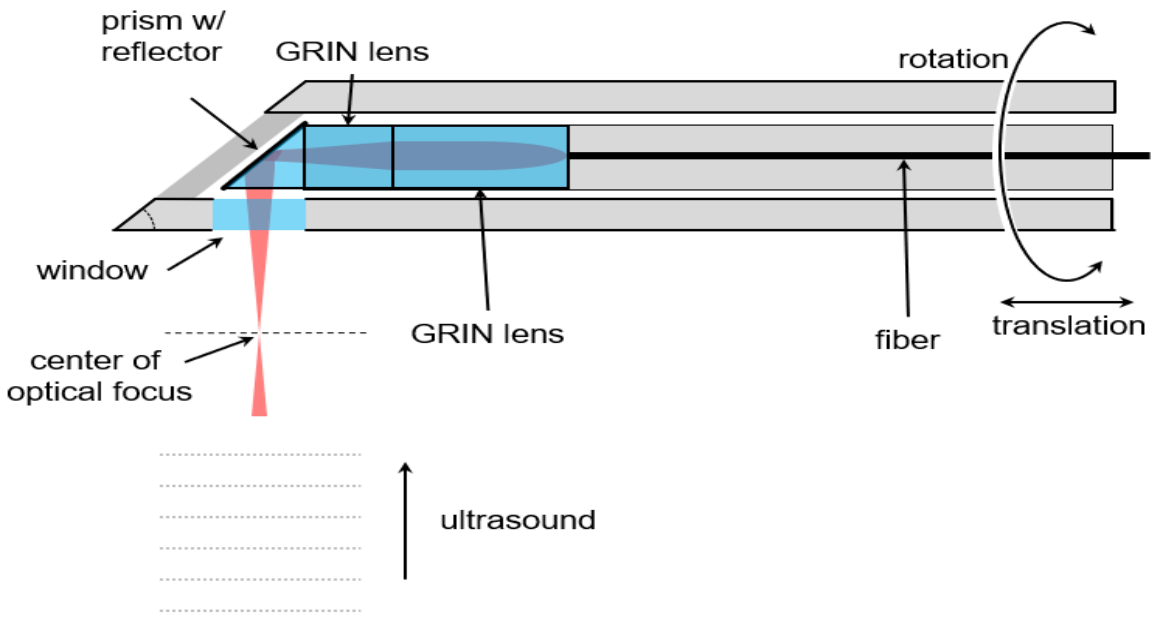

Figure 1. *The schematic diagram of our endoscope housed within a 21-gauge needle.*

To proceed building the endoscope, we needed to first determine the optimal GRIN lens length to give us a focal length between 0.5 and 1 mm. This focal length will help achieve the desired depth when used to image cartilage in a spatially constrained joint. It was assumed that the light's dispersal pattern in the lens would be sinusoidal in nature. Each individual lens was a quarter pitch. It was assumed that a single lens would attached to a fiber would collimate the light, and that a full half pitch would refocus the light at the face opposite the fiber. The radius of the lenses is 175 µm and the length of an individual lens is 780µm. Snell's law and the

sinusoidal nature of the light path were taken into account to calculate the approximate the focal length. The generalized equation relating focal length, f, to the lens length, L, is given below.

$$f = 175\sin(R\pi)tan(\arcsin(\frac{n_{GRIN}\sin(\pi - \cos(R\pi))}{n_{AIR}}))$$

$$L = R * 1.56\, mm$$

The refractive index of air, n_{air} is assumed to be 1. The refractive index of the lens, n_{GRIN}, was assumed to be constant because no documentation could be found from the manufacturer. For n_{GRIN}, we used a value based on the material it was made of, which is alumoscilate glass. Wray et al. found the index of refraction at 1367 nm and 1127 nm to be 1.534 and 1.536 respectively. Due to the little variance, n_{GRIN} was estimated to be 1.53. With these known values, we could calculate the total length of GRIN lenses needed to achieve the desired focal distance. Lenses were then ground down to approximately this length and the focal length was tested using a 1300 nm laser.

Needles used for lens alignment were cut in half and thinned by hand such that they could be inserted into an unaltered needle. In addition to fabricating the endoscope housing we also designed a needle holding apparatus with a radius of 31.75 mm that will keep the endoscope steady while it is being rotated[7]. This diameter was chosen due to the low power loss expected as demonstrated in Figure 2. We designed our needle holder using Solidworks and then 3D printed it using the Dimension Elite 3D printer. The rat stage was fabricated using plexiglass and the Joint stabilizing stage was also designed in Solidworks and 3D printed using the same printer.

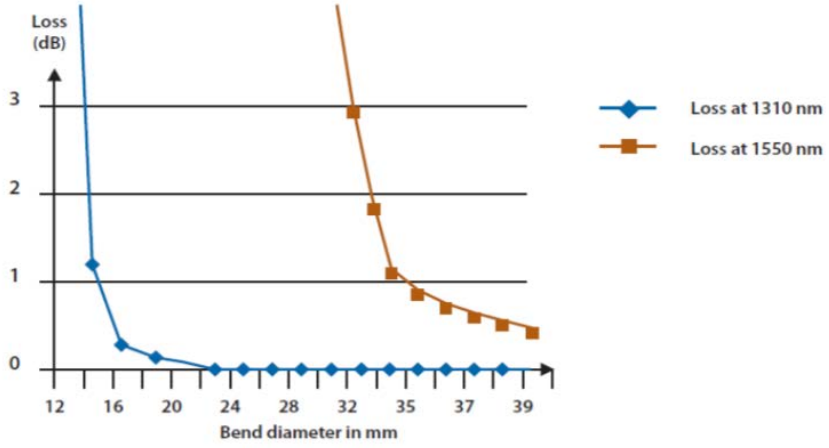

Figure 2. *Graph depicting the loss of power for varying diameter at both 1310 nm and 1550 nm. Our system will be using 1310 nm with a bending diameter of 63.5 mm.*

2.2 Mobility of the Device

In addition to the endoscope itself, an apparatus had to be build that would allow the endoscope to move and rotate inside of the body. To accomplish this, two motorized systems were incorporated. The first component of locomotion is the translational stage which is used to move the endoscope back and forth, giving us the ability to look at different regions in a joint. We used the KMTS50E motorized translational stage made by Thorlabs and its corresponding software.

The second component of locomotion is a rotational motor assembly which gives the ability to view the entire joint by rotating the endoscope 360 degrees. The assembly consists of a BLY17MDCUSB series DC motor made by Anaheim Automation with a great attached to the shaft of the motor. The fiber connecting to the endoscope is connected to a joint that allows for the fiber to rotate freely. This joint is held inside of a bearing with an area cutout such that one end of the joint is forced to rotate along with the bearing. Connected to the bearing is a gear that can meet to the shaft of the motor. A chassis holds the bearing and motor in place such that both gears can meet up allowing for the endoscope fiber to be rotated by the motor. A rear plate holds

the back half of the rotational joint (connecting to the optical system) fixed to the chassis. A Needler Holder was also designed that allowed us to hold the endoscope in place, store excess cabling, as well as a bulk head used to connect the rotatory joint and endoscope. Around the shaft of the Needle Holder, we also connected a M15H magnetic encoder from Timken. The magnetic encoder allows for angular position and angular velocity measurements. Although we pre-set the rotational motor's speed using software from the manufacturer Anaheim Automation, there is some variation in the actual values. These angle and angular velocity measurements are used for the post-processing of data as they give us the actual angle, angular velocity, and time any given pixel was obtained.

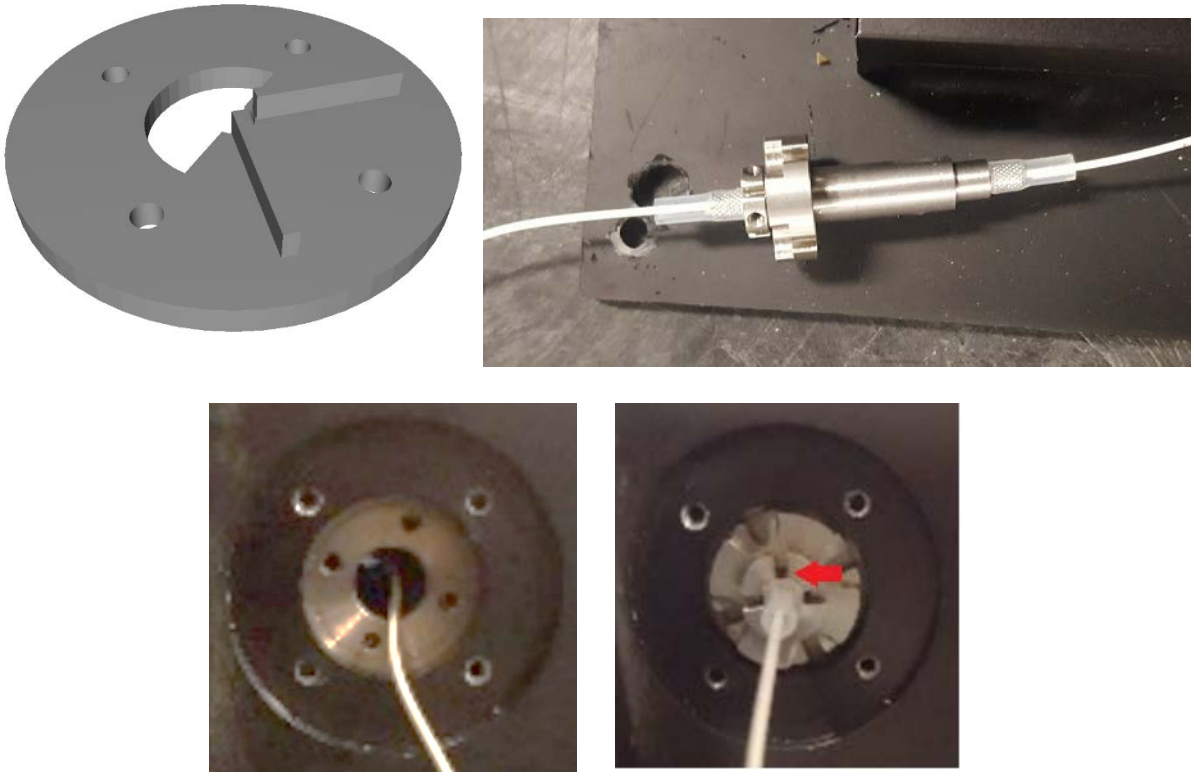

Figure 3. *The top right image is a photo of the rotational joint that we used. It allowed for one side of the fiber to be rotated (left), while the other side was held in place by the rear cap (top left) that bolted into the chassis. The rear cap has 2 fins that can fit into grooves in the rotational*

joint. It also has 4 holes allowing for it to be bolted to the chassis. The bottom left photo was taken of the bearing prior to the insertion of the rotational joint. The bottom right image shows the joint inserted and has an arrow pointing to where the fins of the rear plate as inserted.

Figure 4*. This is a photo taken of the top view of our gear system. The gear on the right connects to the motor's shaft. The larger gear on the left is connected to a bearing housed within the black metal Chassis. This surrounds the rotary joint and controls the speed at which the endoscope rotates.*

2.3 Design Prototype

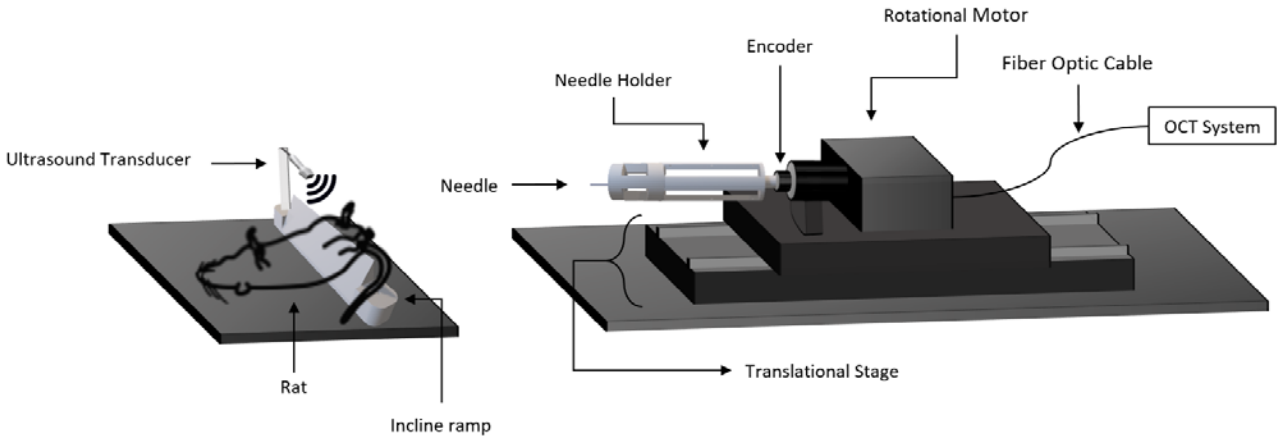

Figure 5. *This is the overall layout of our device design. The rat will be mounted and strapped down to a mounting platform (pictured on the left). The rat's knee will arch*

over the ramp and bend it at a 35° angle to ensure maximal exposure of the synovial space[8].

3. Theory Implementation

The ability to gather elastographic data from our system is reliant on ultrasound. An ultrasound transducer is set up abutted to the rat joint and gives us the ability to perturb the cartilage within the joint. The ultrasound transducer was controlled by a function generator, specifically the function generator component of the National Instruments Virtualbench device. Noting that osteoarthritic cartilage is stiffer than normal cartilage, we expect to see a higher Young's modulus when calculated from an OCE image of an osteoarthritic joint than a healthy joint. The contrast medium we will be using to view the joint is composed of two states: when ultrasound is on, and when ultrasound is off. This contrast medium is necessary as it enables us to visualize the mechanical properties, specifically the Young's modulus, of a joint by comparing imaging data gathered when it is being stimulated by ultrasound with when it is static. The actual processing method that allows for mechanical properties to be measured from OCT images is still under development.

3.1 Triggering Function and Post-Processing

The initialization of the individual components are all based off of a trigger signal output by the OCT system's. This trigger corresponds with the system's data acquisition and is normally used to control mirror galvanometers in conventional imaging through air. The trigger enables us to start all the individual components as well as data acquisition simultaneously. Figure 5 shows the complete system design with all the individual components and how they are interconnected. The OCT trigger is sent out of the main OCT system and triggers the function generator of the Virtualbench to send out a waveform that triggers the ultrasound transducers to

be periodically turned on and off. The ultrasound then stimulates the cartilage within the rat joint and the images of the cartilage are taken by the endoscope. The endoscope sends light into the cartilage at different areas and angles of the joint via the translational stage and rotational motor and detects the light reflected. This reflected light then travels back through the endoscope and to the OCT system via optical fiber where the imaging data is stored for post processing.

3.2 Ultrasound Transducer Stimulation

$$f_o = \frac{1}{\left(\left(\frac{DC_i}{100 * f_{in}}\right) 2RE_{on} - 1\right) + \left(\left(\frac{DC_i}{100 * f_{in}}\right) 2RE_{off} - 1\right)}$$

$$DC_o = \frac{\left(\left(\frac{DC_i}{100 * f_{in}}\right) 2RE_{on} - 1\right)}{\left(\left(\frac{DC_i}{100 * f_{in}}\right) 2RE_{on} - 1\right) + \left(\left(\frac{DC_i}{100 * f_{in}}\right) 2RE_{off} - 1\right)} * 100$$

$f_o = Output\ Frequency$
$DC_i = Input\ Duty\ Cycle$
$f_{in} = Input\ Frequency$
$RE_{on} = Number\ of\ Rising\ Edges\ Transducer\ will\ be\ on$
$RE_{off} = Number\ of\ Rising\ Edges\ Transducer\ will\ be\ off$
$DC_o = Output\ Duty\ Cycle$

Figure 6. *These are generalized equations that control when the ultrasound transducer is triggered. The transducer is triggered based on the OCT system's output trigger signal. The OCT system frequency and duty cycle are generalized so that these values can be changed in the system.*

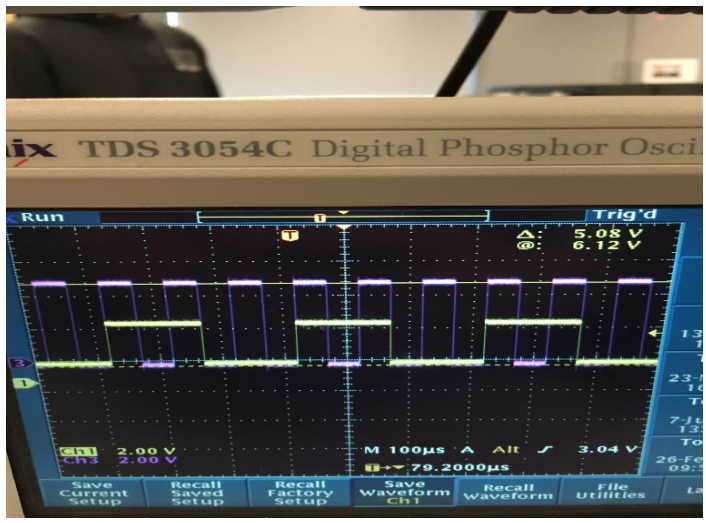

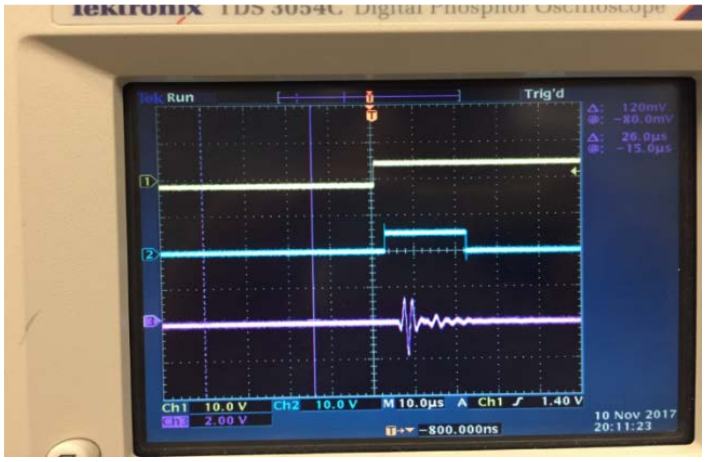

Figure 7. *Top image shows the OCT Computer Output Signal (Purple trace) and the virtualbench output signal (Yellow trace). In this configuration the parameters in the formula above were set to fin = 10kHz, DCi = 50%, REon = 2, REoff = 2. As shown in the figure the virtualbench output is on for 2 OCT Computer Output Signal rising edges and off for 2 OCT rising edges. Bottom image shows OCT trigger (Yellow trace), Ultrasound stimulation signal (Blue trace), and Ultrasound receiver waveform (Purple trace).*

The ultrasound transducer stimulation is based off a signal that is triggered by the OCT output trigger. An equation was derived for determining the ultrasound transducer stimulation signal frequency, which would control how frequent and the specific times the transducers would be on and off, by accounting for the OCT trigger frequency, duty cycle, and the number of rising and falling edges desired to include in one period of ultrasound transducer stimulation signal.

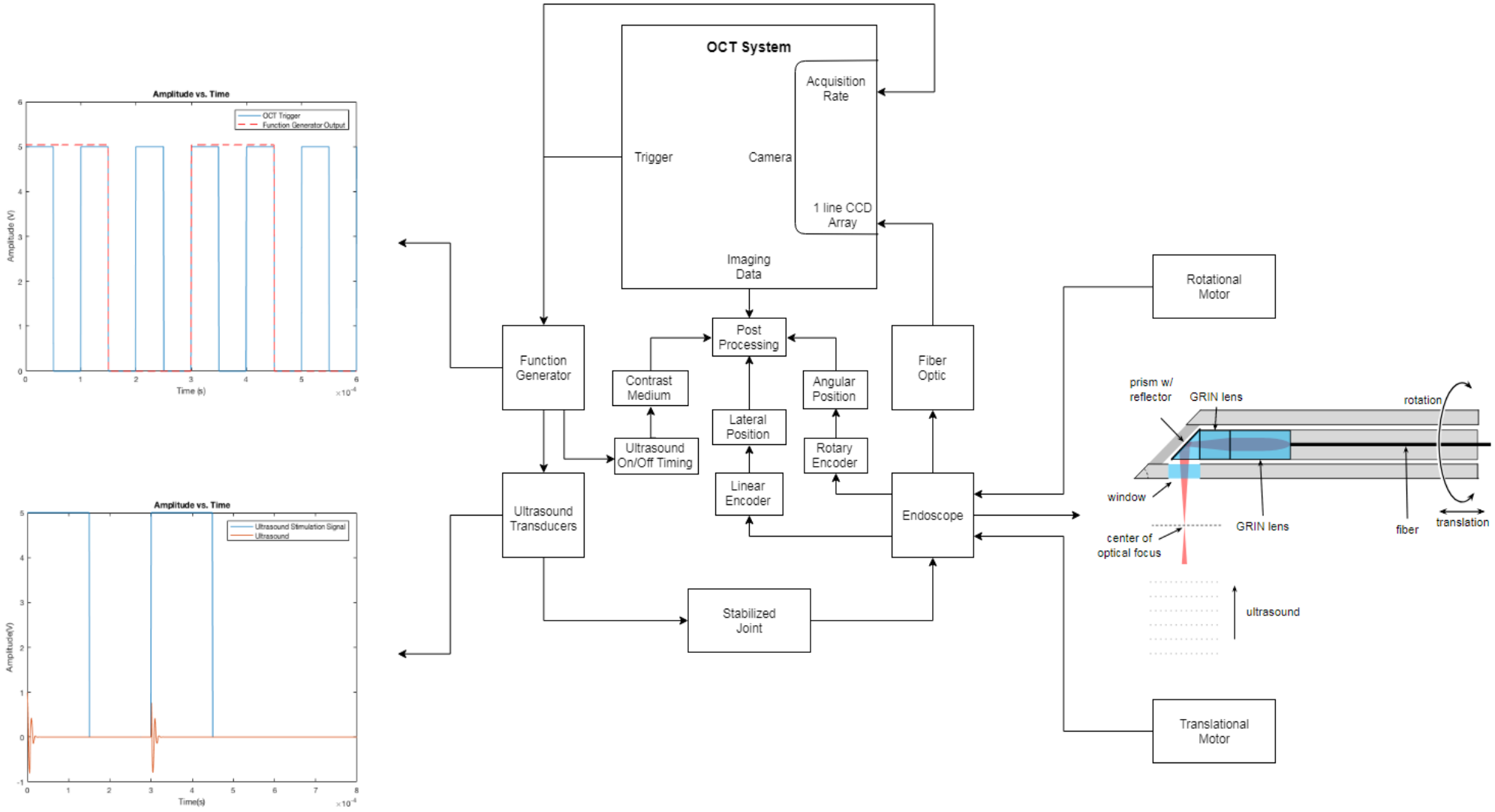

Figure 8. *This figure displays all interconnections of our endoscope system.*

4. Proof of Functionality

4.1 Proof of Concept

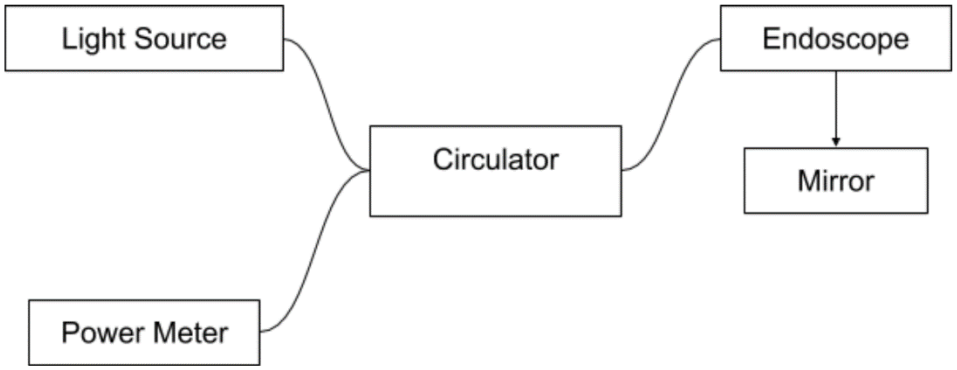

Figure 9. *This diagram shows the experimental set-up we used to test net power loss throughout the endoscope. A light source was connected to port 1 of an optical circulator. Port 2 was connected to the endoscope. The beam from the endoscope was aimed at a mirror. A power meter was connected to Port 3 to measure the power output after the light is sent through the endoscope and back.*

To test the viability of our endoscope, we needed to perform an experiment to view power loss. We gathered data using the setup described in figure 8. We assumed that the used power through a normal fiber as the expected or maximal power we should expect. Using the formula dB = 10*log(Pout/Pin), where Pout is 4.01mW which is the power of light measured through the fiber that goes through the rotary chassis and endoscope and Pin is 7.36mW which is the power of light measured through a regular fiber. We obtain a 2.6dB power loss across the rotary chassis in one direction and about a 5dB power loss across the rotary chassis in both forward and reverse direction as the light will be travelling from the rotary chassis to the endoscope and then back through the rotary chassis. This power loss is relatively low and thus we can say that the fiber through the rotary chassis is good to use for imaging.

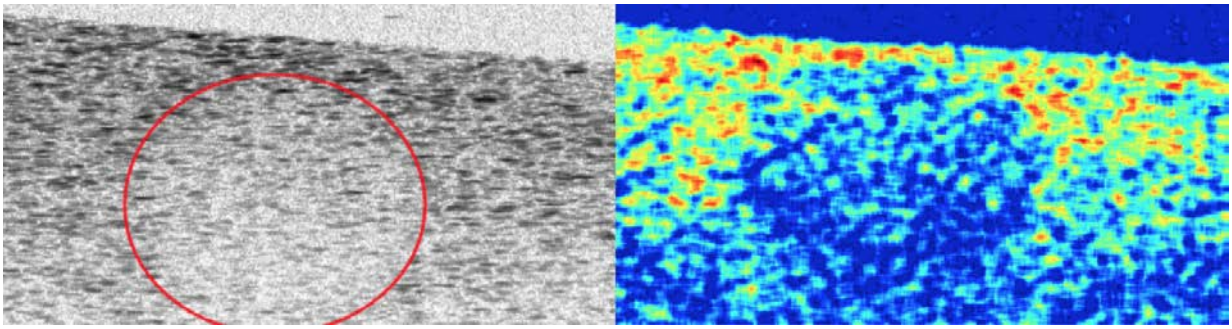

Figure 10. *Sample data of 2% agar surrounding an 8% agar sphere. The left is OCT while the right image is OCE.*

The next proof of concept pertains to elastography. The figure above shows a sphere of 8% agar suspended in 2% agar. The sphere is outlined by the red circle. Using conventional OCT scans through air, one cannot easily make out the 8% from 2% agar. When the same area is scanned while utilizing OCE, we can discern the sphere from its surroundings based on its higher Young's modulus. The technique is still under development and is intended to be used in conjunction with the endoscope to measure the mechanical properties of tissue in the body while also gathering conventional OCT images.

5. Conclusion and Future works

The goal of this project was to develop an endoscopic imaging system that would allow for intra-joint imaging and also the measurement of the mechanical properties of the imaged tissue. This would allow for in vivo imaging and quantification of joints afflicted with diseases such as osteoarthritis. We have shown that a significant amount of light can be passed through our endoscope. The motor systems for the endoscope have also been built and connected to the OCT system allowing the motor system and the endoscope to work in unison. As of now, the OCE imaging capabilities of our system are still under development. We plan to work alongside

a laboratory at the University of Southern California to build an ultrasound transducer that would provide enough ultrasound power to the area that we intend to image.

Once complete, this device will be used in trials to image the joints of mice as osteoarthritis develops. This will allow for greater insight into the progression of the disease. This same technique can be applied to other research such as implants and biomaterials. Our systems will serve as a minimally invasive method to monitor the visual and mechanical properties of a joint with a broad range of different applications.

6. References

1. Spector, T. D., and D. J. Hart. "How serious is knee osteoarthritis?." Annals of the rheumatic diseases 51.10 (1992): 1105.

2. Pollard, T. C. B., et al. "Treatment of the young active patient with osteoarthritis of the hip: a five-to seven-year comparison of hybrid total hip arthroplasty and metal-on-metal resurfacing." Bone & Joint Journal 88.5 (2006): 592-600.

3. Guilak, Farshid. “Biomechanical Factors in Osteoarthritis.” *Best practice & research. Clinical rheumatology* 25.6 (2011): 815–823. *PMC*. Web. 14 May 2018.

4. Tearney, Guillermo J., et al. "In vivo endoscopic optical biopsy with optical coherence tomography." Science 276.5321 (1997): 2037-2039.

5. Verzijl, Nicole, et al. "Crosslinking by advanced glycation end products increases the stiffness of the collagen network in human articular cartilage: a possible mechanism through which age is a risk factor for osteoarthritis." Arthritis & Rheumatology 46.1 (2002): 114-123.

6. Manickam, Kavitha, Ramasubba Reddy Machireddy, and Suresh Seshadri. "Characterization of biomechanical properties of agar based tissue mimicking phantoms for ultrasound stiffness imaging techniques." Journal of the Mechanical Behavior of Biomedical Materials 35 (2014): 132-143.

7. Salleh, M. F. M., Salleh, Zakaria, Z. (2015). Optical Fiber Bending Detection on Long

8. Distance OPGW using OTDR. Telkomnika, 13(3), 889-893.

9. Glasson, S. S., et al. "The OARSI histopathology initiative–recommendations for histological assessments of osteoarthritis in the mouse." Osteoarthritis and cartilage 18 (2010): S17-S23.

10. “CPC Definition - A61B DIAGNOSIS; SURGERY; IDENTIFICATION (Analysing Biological Material G01N, e....” *United States Patent and Trademark Office - An Agency of the Department of Commerce*, www.uspto.gov/web/patents/classification/cpc/html/defA61B.html.

11. “Osteoarthritis Diagnosis.” *Www.arthritis.org*, Arthritis Foundation, www.arthritis.org/about-arthritis/types/osteoarthritis/diagnosing.php.

12. “US FDA Registration Process for Medical Devices.” *Emergo*, 17 July 2017, www.emergobyul.com/resources/usa-process-chart.

13. Medicaid.gov. (2018). *List of Medicaid Benefits | Medicaid.gov.*, https://www.medicaid.gov/medicaid/benefits/list-of-benefits/index.html.

[13] eHealthMedicare. (2018). *Medicare Coverage: Benefits Covered by Medicare*. https://www.ehealthmedicare.com/medicare-coverage-articles/medicare-coverage/.

14. Zhang, Y. and Jordan, J. (2010). *Epidemiology of Osteoarthritis*, 26(3), pp.355-369.